Fatigue resistance of basalt fibers-reinforced laminates

A Dorigato and A Pegoretti

Journal of Composite Materials 2012 46: 1773 originally published online 15 May 2012
DOI: 10.1177/0021998311425620

Article

JOURNAL OF COMPOSITE MATERIALS

Journal of Composite Materials
46(15) 1773–1785

DOI: 10.1177/0021998311425620
jcm.sagepub.com

SAGE

Fatigue resistance of basalt fibers-reinforced laminates

A Dorigato and A Pegoretti

Abstract

Fabrics of basalt (BFs), E-glass (GFs), and carbon (CFs) fibers with the same areal density were used to prepare epoxy-based laminates. The BF laminates presented elastic moduli and strength values higher than those of the corresponding GF laminates, with tensile strength values near to that of CF laminates. Investigation of the behavior under fatigue conditions indicated superior performances of BF laminates with respect to the corresponding GF composites, with an improved capability of sustaining progressive damaging and slightly higher damping properties. As far as the fatigue behavior is concerned, BFs may therefore represent a valid substitute of GFs in structural composites.

Keywords

Polymer–matrix composites (PMCs), basalt fibers, fatigue

Introduction

Fiber-reinforced polymers (FRPs) offer several attractive features for various engineering sectors, including high performance, light weight, and reduced life cycle costs.[1] Basalt fiber (BF) has recently gained an increasing attention as possible replacement for traditional glass and carbon fibers (CFs) in FRPs.[2–5] The term basalt indicates a variety of dark volcanic rocks, formed by solidified lava.[6–8] Though basalt stones are available in various compositions, only certain types are suitable for the production of technical filaments. In particular, basalt rocks with silicon dioxide (SiO_2) content of about 46% (acid basalt) can be utilized for fiber production.

After the first patent revealing the technique of producing the BF, the greatest part of the research was carried out in Russia and Czech Republic.[8] Technological process of basalt filaments manufacturing consists of melt preparation, fiber extrusion, application of sizing agents, and final winding. The density of the BFs (from 2.5 to 2.9 $g \cdot cm^{-3}$) is very much lower than metals and closer to that of glass fibers. Compared to glass fibers, BFs are characterized by an elevated resistance against alkaline environment, while relatively less stability has been registered in strong acids.[9–11] Because of the elevated hardness (from 5 to 9 on Mohr's scale), BFs are characterized by elevated abrasion properties. Due to their excellent thermal properties, BFs can be exposed for hours at 1100–1200°C without any physical damage. Because of these properties, BFs resulted to be attractive for several technological applications, such as geopolymeric concretes,[12] pressure pipes,[13] fibrous insulators,[14] protective clothes,[12–16] and fire-blocking material.[7,17]

Over the last years, BFs have been proposed for the preparation of structural composites in combination with various polymer matrices such as unsaturated polyester,[11] vinylester,[18–22] epoxy,[22–32] phenol formaldehyde,[33–35] polyimide,[36] polysiloxane,[37,38] polypropylene,[39–43] polycarbonate,[41] poly(ethylene terephthalate),[44] poly(butylene terephthalate),[45] polyamide,[46,47] starch resin,[48,49] and polylactic acid.[50] Moreover, BFs have also been used for the preparation of hybrid composites, in combination with more traditional reinforcing fibers such as glass,[51] carbon,[27–32] aramid,[52] and nylon.[29]

Some authors explored the potential of basalt as replacement of E-glass fiber (GF) in reinforced

Department of Materials Engineering and Industrial Technologies and INSTM Research Unit, University of Trento, via Mesiano 77, 38123 Trento, Italy

Corresponding author:
A Dorigato, Department of Materials Engineering and Industrial Technologies and INSTM Research Unit, University of Trento, via Mesiano 77, 38123 Trento, Italy.
Email: andrea.dorigato@ing.unitn.it

polymers.[22,24,26,53] For instance, Liu et al.[24] showed that basalt–epoxy composite had a Young's modulus comparable to that of the glass–epoxy composite reinforced by a twill weave fabrics of nearly identical structure, without significant differences in tensile, flexure, shear, and compression strengths. Wang et al. showed how the interface formed between BF and epoxy resin was better than that of glass fiber and epoxy resin.[26]

Quite surprisingly, only scarce attention has been devoted to the fatigue behavior of BF-reinforced laminates. In a recent work, Wu et al.[32] compared the mechanical behavior of various epoxy composites reinforced with CFs, glass, BFs, and polyparaphenylen benzobisoxazole (PBO) fibers subjected both to monotonic and cyclic loads. It was shown that the fatigue behavior of PBO and basalt was comparable to that of the conventional fibers. Unfortunately, in this manuscript, no information on the areal density of the various fabrics and actual fiber volume fractions were reported.

In the present manuscript, continuous fiber-reinforced laminates were prepared through a hand layup process by using CFs, GFs, and BFs with the same areal density. After a thermomechanical characterization of the constituents, an extensive comparison of the mechanical behavior of the prepared laminates was carried out, with particular attention to their fatigue behavior.

Experimental

Materials

A bicomponent epoxy resin, supplied by Elantas Camattini (Collecchio, Italy), was selected as polymer matrix. In particular, EC152 epoxy base (density of $1.15\,g\cdot cm^{-3}$, viscosity of 1500 mPa·s) and W152 LR amminic hardener (density of $0.95\,g\cdot cm^{-3}$, viscosity of 30 mPa·s) were mixed at a weight ratio of 100/30. Carbon, basalt, and E-glass bidirectional woven fabrics with the same areal density of $200\,g\cdot m^{-2}$, denoted as CF200, BF200, and GF200, were utilized. The CF200 and GF200 fabrics were provided by Model Center S.a.s. (Florence, Italy), while BF200 fabrics were furnished by Aldebran S.p.A. (Bergamo, Italy). Moreover, BFs having a higher areal density of $280\,g\cdot m^{-2}$ (BF280), supplied by R&G Faserverbundwerkstoffe GmbH (Waldenbuch, Germany), were also used.

Characterization of the constituents

The density of the matrix and of the fibers was measured by a Micromeritics Accupyc 1330 helium pycnometer, equipped with a 3.5 cm^3 chamber at a temperature of 23°C.

The glass transition temperature (T_g) of the cured epoxy resin was measured through a TA Instruments MDSC 2920 modulated differential scanning calorimeter (DSC), in the temperature range from 30°C to 180°C at a heating rate of $10°C\cdot min^{-1}$, under a nitrogen flow of $200\,mL\cdot min^{-1}$.

Table 1. Thermomechanical properties of the epoxy resin utilized in this work. T_{g1} and T_{g2} refer to the glass transition temperatures measured during the first and second DSC scan, respectively

Physical property	Value
Density ($g\cdot cm^{-3}$)	1.14 ± 0.01
T_{g1} (°C)	80 ± 1
T_{g2} (°C)	103 ± 1
E (GPa)	2.86 ± 0.03
σ_b (MPa)	70.0 ± 2.3
ε_b (%)	5.3 ± 1.0

DSC: differential scanning calorimeter.

Tensile mechanical properties of neat matrix were measured on ISO 527-1 standard dogbone specimens by using an MTS MiniBionix 858 testing machine equipped with a load cell of 25 kN, at a testing speed of $1\,mm\cdot min^{-1}$. Axial deformation was monitored through an Instron 2620 extensometer, up to a longitudinal strain of 0.3%, while for higher strain levels the longitudinal displacement was determined referring to the crosshead displacement. In this way, the elastic modulus (E), intended as secant modulus between deformation levels of 0.05% and 0.25%, the stress, and the strain at break (σ_b, ε_b) were determined. The thermomechanical properties of the epoxy matrix utilized in this work are summarized in Table 1.

Tensile mechanical properties of the fibers were determined by using an Instron 4502 tensile testing machine, equipped with a 10 N load cell. According to ASTM C1557 standard, single filaments were extracted from the fabrics and glued on paper mounting tabs. Before testing, every specimen was preliminary observed with an Ortholux II POL-BK optical microscope at a magnification of 40×, in order to determine the diameter of the fibers. A crosshead speed of $1\,mm\cdot min^{-1}$ was utilized for all the samples. Three fiber lots with gauge lengths of 15, 30, and 45 mm were tested. In this way, it was possible to estimate the elastic modulus (E) of the fibers by taking the compliance of the measuring system into account (see ASTM C1557). As far as the stress at break (σ_b) values are concerned, a Weibull strength distribution was assumed,[54] whose statistical parameters were determined according to an iterative procedure proposed by Gurvich et al.[55] According to this approach, the cumulative distribution of the stress at break of fibers having a generic length $L = k\cdot L_0$ can be modeled as

$$F(s) = 1 - \exp\left[-\left(\frac{s}{A}\right)^m\right] \quad (1)$$

where $s = \sigma_b \cdot k^{-1/m}$ is a reduced stress, m is a shape parameter and A is a scale parameter. All experimental results on specimens of different size are considered together as a statistically representative population, being A and m parameters evaluated by an iterative least square procedure.[55]

Laminates preparation and characterization

Square laminates with a side of 300 mm were prepared by hand layup. Five impregnated fabric layers were stacked in vacuum Mylar® bags and inserted between the flat metallic moulds of a 10 tons Carver Laboratory press. After degassing, a pressure of about 1 MPa was applied and the laminates were cured under vacuum for 2 h at 50°C and 2 h at 80°C. Samples were designated indicating the type of matrix (Epoxy), followed by the kind of reinforcement and its areal density. As an example, Epoxy-BF200 refers to the laminate reinforced with BFs fabrics having an areal density of 200 $g \cdot m^{-2}$. The actual fiber weight percentage in the laminates (W_f) was determined through thermogravimetric analyses (TGA) performed by a Mettler TG50 apparatus from 30°C to 700°C, at a heating rate of 10°C·min^{-1} under a nitrogen flow of 20 mL·min^{-1}. About 50 mg were tested for each sample. The effective fiber weight fraction in the composites was determined subtracting to the mass residue at 700°C the char content due to matrix degradation, that was previously determined by separate TGA tests on neat epoxy matrix. Starting from the density of the matrix and of the filler (ρ_m, ρ_f) and of their relative weight amounts (W_m, W_f), it was possible to determine the theoretical density of the laminates ($\rho_{c,th}$) in the absence of voids and the volume fraction of the matrix (Φ_m) and of the filler (Φ_f) in the composites

$$\Phi_m = \frac{\rho_{c,th}}{\rho_m} \cdot W_m \text{ and } \Phi_f = \frac{\rho_{c,th}}{\rho_f} \cdot W_f \quad (2)$$

Concurrently, the void volume fraction in the composites (Φ_V) was determined as

$$\Phi_V = \frac{\rho_{c,th} - \rho_{c,\exp}}{\rho_{c,th}} \quad (3)$$

where the experimental density of the composites ($\rho_{c,\exp}$) was assessed by a displacement method in ethanol (Sigma Aldrich, 98% purity) according to ASTM D792 standard.

Quasi-static and fatigue tensile mechanical tests were performed by a MTS Minibionix 858 machine equipped with a 25 kN load cell on rectangular end-tabbed samples 250 mm long and 15 mm wide, milled from the laminates. Quasi-static tests were performed according to ASTM D3039 standard at a crosshead speed of 2 mm·min^{-1}. The deformation was monitored by an Instron 2620 extensometer. In this way, the elastic modulus (E) and the stress and the strain at break (σ_b, ε_b) values were determined. At least 10 specimens were tested for each sample.

Fatigue life tests were carried out according to ASTM D3479 standard applying a 10 Hz sinusoidal stress ranging from a minimum (σ_{min}) stress up to a maximum (σ_{max}) stress, this latter ranging from 10 to 90% of the quasi-static strength. A load ratio $R = \sigma_{min}/\sigma_{max}$ of 0.1 was fixed for all tests. The relative elastic modulus, i.e. the ratio between the elastic modulus measured at a given fatigue cycle (E_N) and the elastic modulus determined in quasi-static tensile tests (E) was measured referring to the crosshead displacement. The specific damping capacity (SDC) was computed as the ratio between the dissipated (W_{diss}) and the total (W_{el}) energy adsorbed at each fatigue cycle, as reported in the following equation

$$SDC = \frac{W_{diss}}{W_{el}} = \frac{\oint \sigma d\varepsilon}{\int_{\varepsilon_{min}}^{\varepsilon_{max}} \sigma d\varepsilon} \quad (4)$$

where ε_{max} and ε_{max}, respectively, represent the maximum and the minimum deformation reached at each fatigue cycle.

Results and discussion

Mechanical characterization of the fibers

The fiber strength distribution is plotted in Figure 1, while the main properties of the selected reinforcing

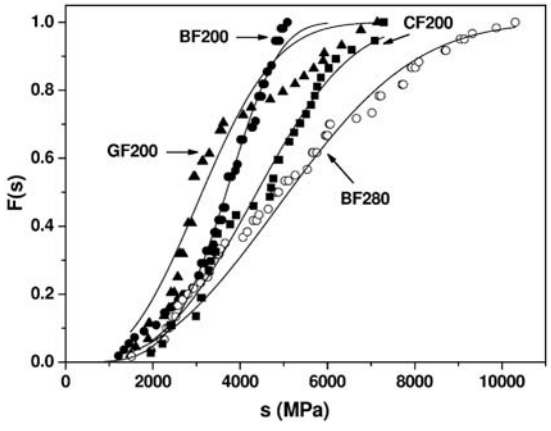

Figure 1. Cumulative distribution function of the reduced stress $F(s)$, with the fitting lines of the experimental data according to Equation (1), ($L_0 = 1$ mm).

Table 2. Density, mean diameter (D) and quasi-static tensile properties at various gauge lengths L of the fibers utilized in this work. E_f is the tensile modulus evaluated according to ASTM C1557, while A and m are the parameters of the Weibull distribution of Equation (1) referred to a gauge length $L_0 = 1$ mm

Sample	Density ($g \cdot cm^{-3}$)	D (μm)	L (mm)	Number of spec.	E (GPa)	E_f (GPa)	σ_b (MPa)	ε_b (%)	A (MPa)	m
CF200	1.73 ± 0.01	8.2 ± 0.4	15	8	183 ± 29	197 ± 10	2136 ± 531	1.08 ± 0.18	4962 ± 40	2.96 ± 0.10
			30	24	201 ± 20		1526 ± 643	0.74 ± 0.27		
			40	9	195 ± 12		1545 ± 620	0.78 ± 0.28		
GF200	2.62 ± 0.01	10.4 ± 0.6	15	8	71 ± 11	67 ± 7	1641 ± 673	2.33 ± 0.84	3583 ± 74	2.70 ± 0.22
			30	28	69 ± 14		1035 ± 402	1.50 ± 0.46		
			40	8	69 ± 6		1202 ± 571	1.73 ± 0.76		
BF200	2.59 ± 0.01	12.3 ± 1.1	15	15	66 ± 5	65 ± 2	1826 ± 617	2.72 ± 0.94	4004 ± 16	4.36 ± 0.12
			30	24	64 ± 4		1586 ± 433	2.46 ± 0.68		
			40	16	67 ± 4		2044 ± 244	3.01 ± 0.40		
BF280	2.62 ± 0.01	20.6 ± 2.2	15	10	103 ± 11	82 ± 6	2277 ± 392	2.22 ± 0.43	5894 ± 57	2.57 ± 0.08
			30	40	82 ± 19		1297 ± 667	1.57 ± 0.74		
			40	10	90 ± 5		1295 ± 510	1.47 ± 0.61		

fibers are summarized in Table 2. As expected, the density of BFs is practically equal to that of GFs and considerably higher than that of CFs. While elastic modulus of BF200 filaments is similar to that of GF200 fibers (in the range 65–67 GPa), the stiffness of BF280 sample is remarkably higher (82 GPa). It is therefore confirmed that the elastic modulus of BF does markedly depend on their chemical composition, being generally slightly higher than that of GFs.[53,56] On the other hand, tensile strength of BF is much higher than that of GF fibers, with values comparable to or even higher than that of CF. The resulting scale (A) and shape (m) parameters of the Weibull strength distribution are also reported in Table 2. The cumulative strength distribution of the investigated fibers is reported in Figure 1. The continuous fitting lines have been drawn on the basis of the Weibull distribution of Equation (1), at a reference length (L_0) of 1 mm. The appropriateness of the Weibull distribution in fitting the strength data is supported by a coefficient of determination (R^2) higher than 0.92. The mean tensile strength of the fibers ($\bar{\sigma}_b$) can be expressed as[57]

$$\bar{\sigma}_b = A\left(\frac{L}{L_0}\right)^{-\frac{1}{m}} \Gamma\left(1+\frac{1}{m}\right) \tag{5}$$

where Γ is the gamma function. It is worthwhile to note that strength data obtained on single basalt filaments are relatively scarce in the scientific literature.[23,53,56,58,59] Our data are in rather good agreement with the parameters of the Weibull strength distribution reported by Park et al.[23]

Table 3. Density, fiber volume fraction (Φ_f) and void content (Φ_V) of the investigated laminates

Sample	Thickness (mm)	Density ($g \cdot cm^{-3}$)	Φ_f (%)	Φ_V (%)
Epoxy-CF200	0.89 ± 0.02	1.51 ± 0.01	63.5	0.15
Epoxy-GF200	0.72 ± 0.02	1.92 ± 0.01	56.3	2.56
Epoxy-BF200	0.68 ± 0.02	1.98 ± 0.02	61.3	2.33
Epoxy-BF280	1.01 ± 0.03	1.86 ± 0.02	54.1	4.13

Preliminary characterization of laminates

Thickness, density, fiber volume fraction, and void content of the investigated laminates are summarized in Table 3. For composites reinforced with fabrics having the same areal weight of 200 $g \cdot m^{-2}$, the fiber volume fraction are quite similar. For as concerns the void content, CF-reinforced laminates are characterized by the lowest value (0.15 vol%), probably because of the better fiber wettability with the selected epoxy matrix. The BF and GF laminates are characterized by similar void contents in the range 2.3–2.6 vol%. For Epoxy-BF280 laminates, an elevated void content (more than 4 vol%) has been determined, probably because more air was entrapped in the heavier fabrics during the hand layup process.

Quasi-static tensile mechanical properties of the investigated laminates are summarized in Table 4. As expected, Epoxy-CF200 laminate shows the highest elastic properties, the highest stress at break, and the lowest strain at break values. Interestingly, the stiffness

Table 4. Quasi-static tensile properties of the investigated laminates

Sample	*E* (GPa)	σ_b (MPa)	ε_b (%)
Epoxy-CF200	65.1 ± 5.3	728 ± 67	1.1 ± 0.2
Epoxy-GF200	25.2 ± 2.1	461 ± 25	2.3 ± 0.2
Epoxy-BF200	29.6 ± 2.7	600 ± 36	2.6 ± 0.2
Epoxy-BF280	26.5 ± 1.9	502 ± 26	2.4 ± 0.2

of Epoxy-BF200-reinforced composites is 20% higher than that of Epoxy-GF200, and also, the stress at break is considerably higher (30% higher than Epoxy-GF 200 sample). Considering that strain at break of GF and BF samples are similar (about 2.5%), it emerges a potential for BFs in replacing traditional GFs in structural composites. Even if quasi-static tensile properties of BF280 filaments are better than that of BF200 fibers, it is interesting to note that elastic moduli of the above mentioned composites are quite similar. A modelization of the elastic modulus of BF200 and BF280 composites was attempted on the basis of a theoretical approach proposed by Hofstee and van Keulen (not reported in the article for the sake of brevity).[60] This model is more sophisticated than the classical lamination theory and takes stiffness reduction due to fiber crimping into account. Considering that an elastic modulus value of 27.3 GPa was found for both the composites, it could be concluded that theoretical results are very near to those found experimentally. Moreover, it is interesting to note that the tensile stress at break of Epoxy-BF280 laminate is lower than that of the corresponding BF200 composite sample. This discrepancy could be probably explained considering the lower fiber content and the higher voids amount of Epoxy-BF280 laminate.

Fatigue resistance of laminates

Maximum tensile stress-*N* fatigue curves of the investigated composites are reported in Figure 2(a). It is immediately evident the relatively low fatigue sensitivity of CF200 laminate, while the higher tensile strength of BF200 with respect to GF200 is responsible for the better fatigue performance of the basalt laminate. Once again, the fatigue behavior of BF280 composite is heavily affected by the higher void content and the lower fiber amount with respect to the BF200 sample. It can be now interesting to model fatigue data of the tested laminate by using a theoretical approach. As often reported in literature,[61] fatigue curves of composite materials can be fitted with the following equation

$$\sigma_{\max} = \mathrm{B} \cdot N^{-\frac{1}{k}} \tag{6a}$$

This can be linearized in a double logarithmic scale

$$\log(\sigma_{\max}) = \log(B) - \frac{1}{k} \cdot \log N \tag{6b}$$

Fatigue plots in double logarithmic scale, with the fitting lines according to Equation (6b), are represented in Figure 2(b), while the fitting parameters are collected in Table 5. It can be important to underline that fitting of fatigue data was carried out without considering the points corresponding to the quasi-static conditions. A linear trend is followed by all the tested samples, and the low fatigue sensitivity of the CF200 is reflected in the higher value of the *k* parameter. A certain discrepancy can be noticed between the *B* values and the quasi-static tensile strength of the tested composites (see Table 5). This is probably due to the different loading conditions adopted in quasi-static and fatigue tests.

Normalized *S–N* fatigue curves are reported in Figure 2(c) for all the considered laminates. The CF-reinforced laminates display the highest fatigue resistance, while the trend shown by Epoxy-BF200 composites is similar to that observed for Epoxy-GF200 composites. However, it has to be taken into account that quasi-static tensile strength of BF200 laminates is roughly 30% higher than that of Epoxy-GF200 composites. Analyzing a great amount of fatigue data, Mandell[62] verified that normalized *S–N* curves of composites with long or short fibers, with various matrices and orientation can be reasonably well fitted by the following equation

$$\frac{\sigma_{\max}}{\sigma_b} = 1 - b \cdot \log N \tag{7}$$

Fitting the experimental data with Equation (7) furnishes the *b* parameters reported in Table 5 along with the coefficient of determination, R^2. A comparison with available literature data indicates that *b* value of glass/epoxy composites (0.17) is slightly higher than those reported in the literature,[63] which are in the range from 0.10 to 0.14. For carbon/epoxy laminates the obtained *b* value (0.08) is in good agreement with values reported in the open literature (0.07–0.09).[64] Even for the epoxy/basalt laminates, the obtained *b* value of 0.17 is higher than the one recently reported by Wu et al. under similar testing conditions (0.07).[32] The observed discrepancy with literature data can be explained by considering that the *b* parameter is highly dependent on the fiber volume content,[63] the void content,[65] and the fiber orientation of the composite specimens and on the testing conditions, such as the test frequency.[64]

Nevertheless, the relatively low R^2 values indicate that the selected fitting function is not able to carefully

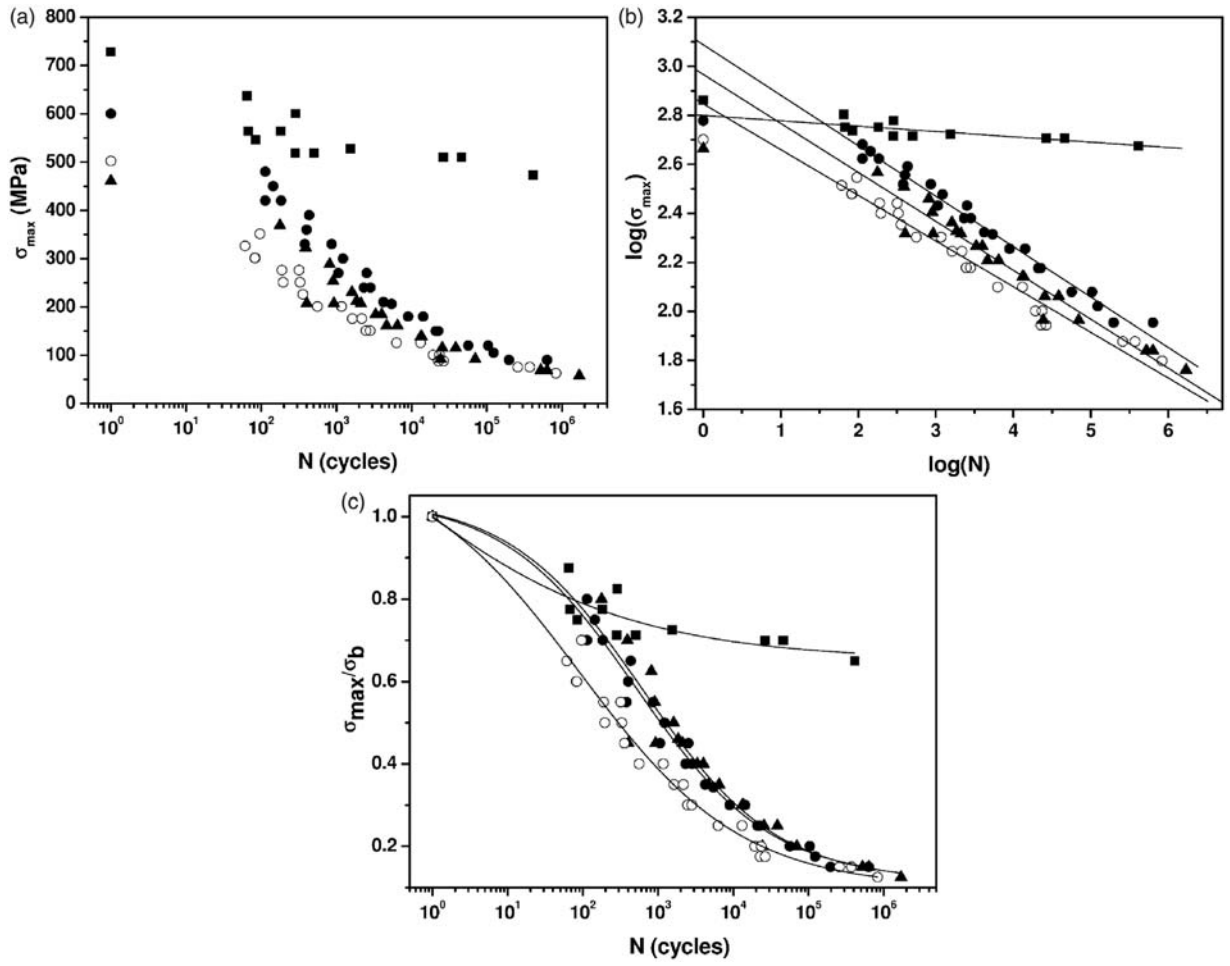

Figure 2. (a) Maximum stress – N curves from fatigue tests on (■) Epoxy-CF200, (●) Epoxy BF200, (▲) Epoxy-GF200, and (○) Epoxy-BF280 laminates. (b) Fatigue data in double logarithmic scale, with the fitting lines according to Equation (6). (c) Normalized stress – N curves with the fitting lines according to Equation (8).

Table 5. Fitting parameters of the fatigue curves of the composite laminates according to Equations (6)–(8)

Sample	B (MPa)	k	R^2	b	R^2	A_1	A_2	N_0	p	R^2
Epoxy-CF200	630 ± 28	45.4 ± 12.4	0.602	0.08 ± 0.01	0.50	1.66 ± 6.05	0.65 ± 0.11	0.1 ± 3.5	0.26 ± 0.56	0.836
Epoxy-GF200	925 ± 89	5.0 ± 0.3	0.983	0.17 ± 0.01	0.96	1.05 ± 0.04	0.12 ± 0.03	514.0 ± 110.8	0.49 ± 0.05	0.984
Epoxy-BF200	1222 ± 62	4.8 ± 0.1	0.946	0.17 ± 0.01	0.94	1.05 ± 0.08	0.12 ± 0.05	621.3 ± 246.9	0.48 ± 0.10	0.942
Epoxy-BF280	702 ± 44	5.4 ± 0.2	0.964	0.19 ± 0.01	0.83	1.14 ± 0.08	0.10 ± 0.03	90.3 ± 34.8	0.40 ± 0.05	0.981

follow the actual trend of the experimental S–N data. Among the various forms proposed to model the stress/life curves of fiber-reinforced composites,[66] a logistic sigmoidal curve has shown good fitting capabilities for fabrics[67] and braided composites.[68] In particular, a Boltzmann sigmoidal function in the following form can be adopted[69]

$$\frac{\sigma_{\max}}{\sigma_b} = A_2 + \frac{A_1 - A_2}{1 + \left(\frac{N}{N_0}\right)^p} \tag{8}$$

where A_1, A_2, N_0, and p are the parameters in the equation. In particular, A_1 and A_2 represent the upper and the lower fatigue stress limits, respectively, while N_0 is the fatigue life for a stress equal to $(A_1 + A_2)/2$. The values of the parameters derived from the fitting of fatigue data according to Equations (7) and (8) are collected in Table 5. It can be immediately noticed that R^2 values associated to linear fitting are lower than that obtained applying sigmoidal expression. In Figure 2(c), the fatigue data of all the tested specimens are fitted by using Equation (8). The efficacy of logistic sigmoidal function

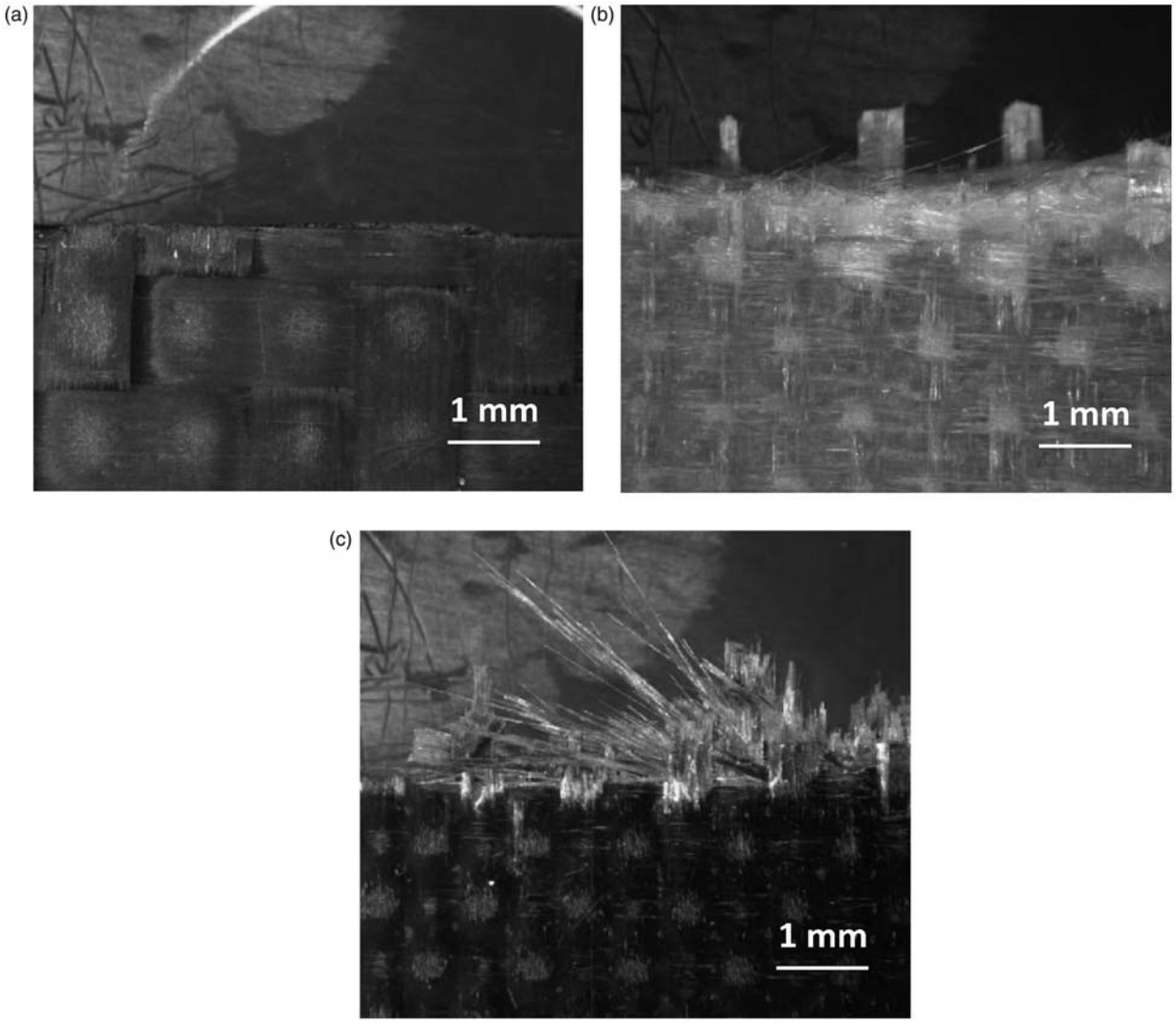

Figure 3. Photographs of the fractured samples in fatigue tests. (a) Epoxy-CF200, (b) Epoxy-GF200, and (c) Epoxy-BF200.

in predicting fatigue behavior of the laminates is confirmed. The highest fatigue resistance and the limited fatigue stress sensitivity of CF200-filled samples results in higher A_2 values (this parameter is generally considered as a fatigue limit of the material). Fitting parameters of Epoxy-BF200 are very similar to those of Epoxy-GF200. In accordance with quasi-static tensile tests, the fatigue resistance of Epoxy-BF200 sample is better than that of BF280 laminate, for which the lower fiber volume fraction and the higher void content determines a reduction of the fatigue limit at elevated fatigue cycles (see A_2 value in Table 5) and a more pronounced fatigue stress sensitivity (i.e. the b parameter in Table 5). While Epoxy-GF200 and Epoxy-BF200 laminates present a similar fatigue behavior and therefore similar N_0 values, the worsening of the fatigue performances encountered for Epoxy-BF200 is reflected in a significant lowering of the N_0 parameter. On the other hand, the N_0 value determined for Epoxy-CF200 composite has solely a mathematical meaning, and it is due to the limited fatigue sensitivity of CF composite.

Photographs collected in Figure 3 show the failure modes of the FRP samples after fatigue failure. The fracture profile of carbon fiber reinforced polymers (CFRP) is very regular, and no fiber debonding can be observed, thus indicating that failure occurs for fiber breakage in the longitudinal direction. Glass- and BF-reinforced laminates show some transversal cracks near the fracture surface and debonding of the fibers belonging to the transversal plies. As suggested by Wu et al.,[32] these observations imply that the fatigue failure mode is markedly influenced by the tensile moduli of the reinforcing fibers. In carbon-reinforced composites, the fatigue stress is effectively transferred along the fibers, while in glass- and basalt-reinforced composites a higher amount of stress is shared with matrix so that transverse

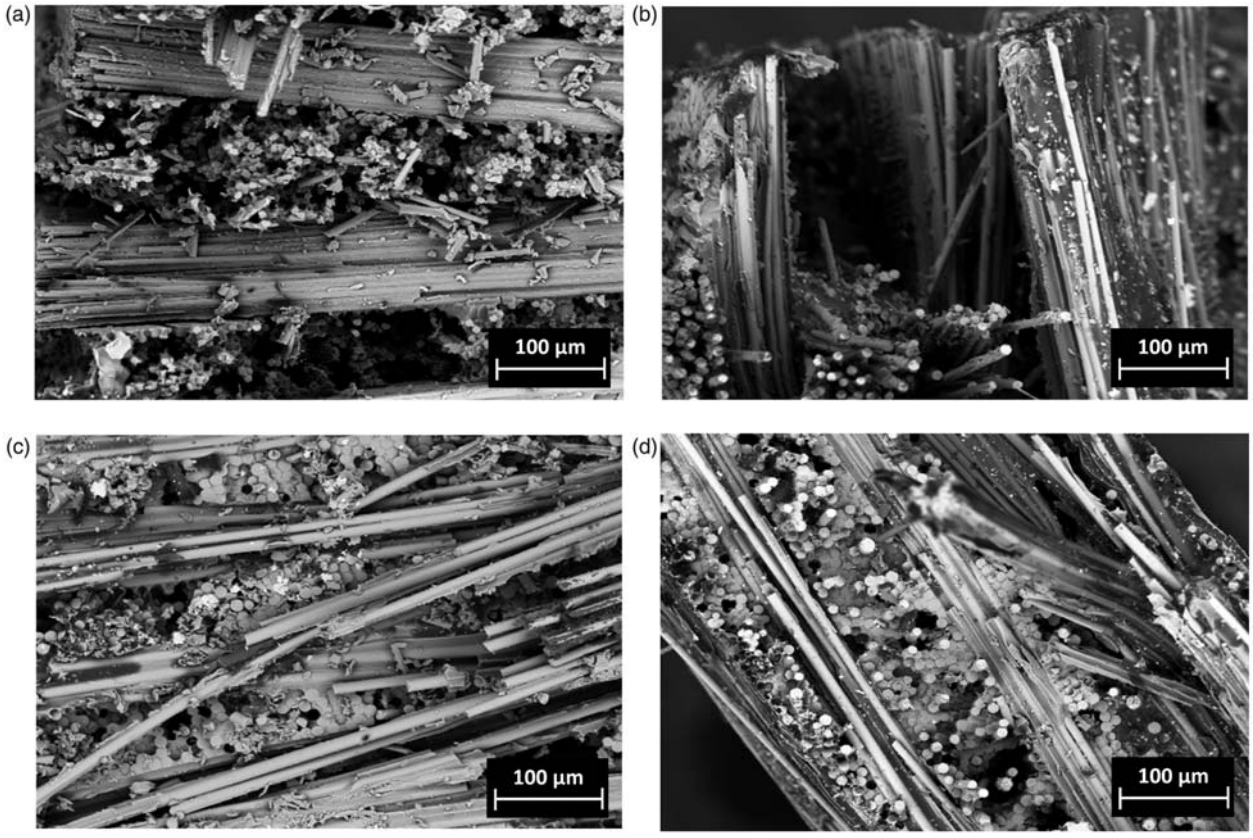

Figure 4. The ESEM micrographs of the fracture surfaces of (a) Epoxy-CF200, (b) Epoxy-GF200, (c) Epoxy-BF200, and (d) Epoxy-BF280 composites.

cracks propagated in the matrix itself, thus favoring transversal delamination phenomena. However, delamination observed in basalt- and glass-reinforced composites could also be attributed to a lower polymer–matrix adhesion with respect to carbon/epoxy composites. In order to support these considerations, environmental scanning electron microscope (ESEM) images of the fracture surfaces of the prepared composites are reported in Figure 4(a)–(d). Even if the differences are not so much pronounced, it can be noticed that in GF and BF composites, debonding phenomena in the transversal direction are present to a higher extent with respect to Epoxy-CF200 sample, confirming therefore the influence of the fiber stiffness on the failure mode of the composites.

It is interesting to analyze the amount of damage accumulated in the laminates during the fatigue test. It is widely recognized that stiffness changes during fatigue loading of composite laminates can be related to produced damages. These variations can be significantly large, and affect deflections, dimensional changes, vibration characteristics, and load stress distributions. Consequently, stiffness is a parameter which could be used to monitor the material damage during its fatigue life.[70] Therefore, the progression of the damage in the selected composites was monitored considering the drop of the relative stiffness (E_N/E) at various fatigue cycles (see Figure 5). As expected, the original stiffness of CF-reinforced composites is maintained over the whole fatigue life if a maximum fatigue stress equal to the 70–80% of the quasi-static tensile strength is applied to the material (Figure 5). As reported in literature,[71] this is generally attributed to the high stiffness of CFs. In these conditions, major part of the applied stress is sustained by the reinforcing fibers without a substantial damage of the matrix, until a catastrophic failure occurs. For lower fatigue stresses, a slight reduction of the material stiffness can be registered (see Figure 5(a) and (b)). It is interesting to note that this decrease is more pronounced in the first part of the fatigue life curve, while for $N/N_b > 0.2$, a decrease of the stiffness loss rate and a subsequent stabilization can be observed. Considering that the main source of stiffness change during the fatigue life of a composite material is matrix cracking in the off-axis plies and that the stiffness drop is proportional to the crack density, it is possible to hypothesize that in the first stages of fatigue test a rapid increase of the crack density occurs, until a stabilization is reached. For BF and GF laminates, a higher degree of damage, with a consequent stiffness reduction, can be observed.

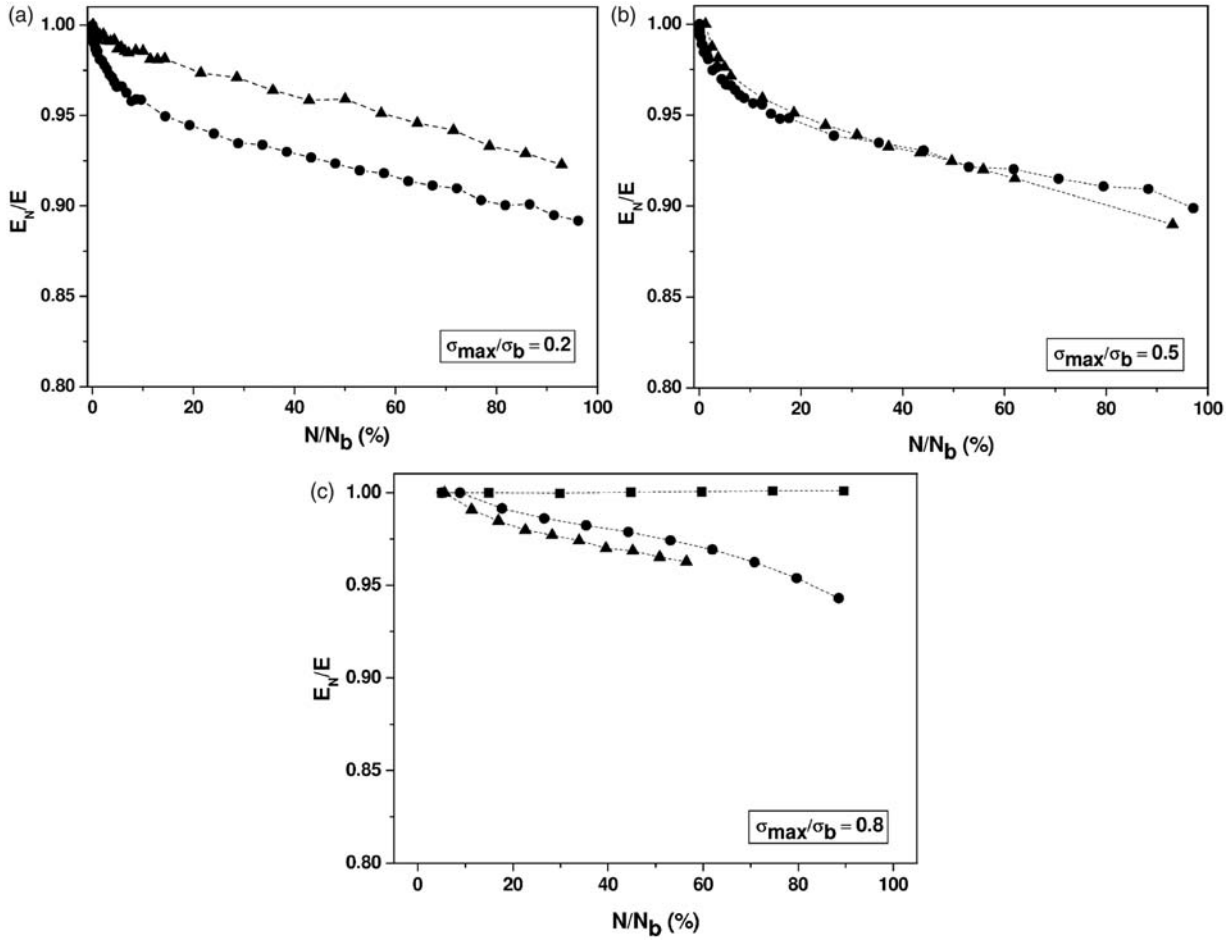

Figure 5. Fatigue behavior of (■) Epoxy-CF200, (●) Epoxy-BF200, and (▲) Epoxy-GF200 laminates. Relative elastic modulus vs. fatigue life at (a) $\sigma_{max}/\sigma_b = 0.2$, (b) $\sigma_{max}/\sigma_b = 0.5$, and (c) $\sigma_{max}/\sigma_b = 0.8$.

At elevated fatigue stresses ($\sigma_{max}/\sigma_b = 0.8$), the damage registered for BF composites is lower than that of GF-reinforced laminates, while the opposite is true if relative stresses lower than 0.5 are considered. It is also interesting to note that at low stress levels, the stiffness loss is higher than that occurring at elevated stress levels; also the stiffness loss gradient is higher. As reported by Razvan et al.,[72] this is probably due to the fact that the damage modes can change primarily in their extent and not in their nature, as the load levels vary. However, in that article, more matrix cracking and delamination was observed in the low-level case at the same fraction of fatigue life, and the final fracture appeared more localized for specimens failed under elevated load levels than under a low load condition, resulting in a more concentrated damage. It is therefore possible to hypothesize that at relatively low fatigue stresses, the crack density in BF composites is higher than that of GF composites, and this aspect could also influence the energy dissipation capability of the samples under fatigue loadings. The damage behavior of BF-reinforced composites at different areal weight is compared in Figure 6(a)–(c). Even if at high fatigue stresses ($\sigma_{max}/\sigma_b = 0.7$), BF280-reinforced composite maintains a higher stiffness than the corresponding BF200 sample, the opposite is observed under low stress levels ($\sigma_{max}/\sigma_b = 0.2$). This means that, while at low stress levels the damaging behavior of BF200 and BF280 composites is similar, at relatively high stresses, BF200 is able to better support matrix cracking and delamination without the occurrence of catastrophic failure. This is probably related to the higher fiber content and lower void fraction of BF200 with respect to BF280 laminates.

Another aspect related to the fatigue behavior of the tested materials is their energy dissipation capability. In Figure 7, SDC values as a function of the relative fatigue stress are reported. Due to the low damping properties of CFs, Epoxy-CF200 laminates show very limited energy dissipation over the whole range of stresses, while SDC values of Epoxy-BF200 sample are 5–10% higher than that showed by the corresponding GF composites. Therefore, it can be concluded that the better

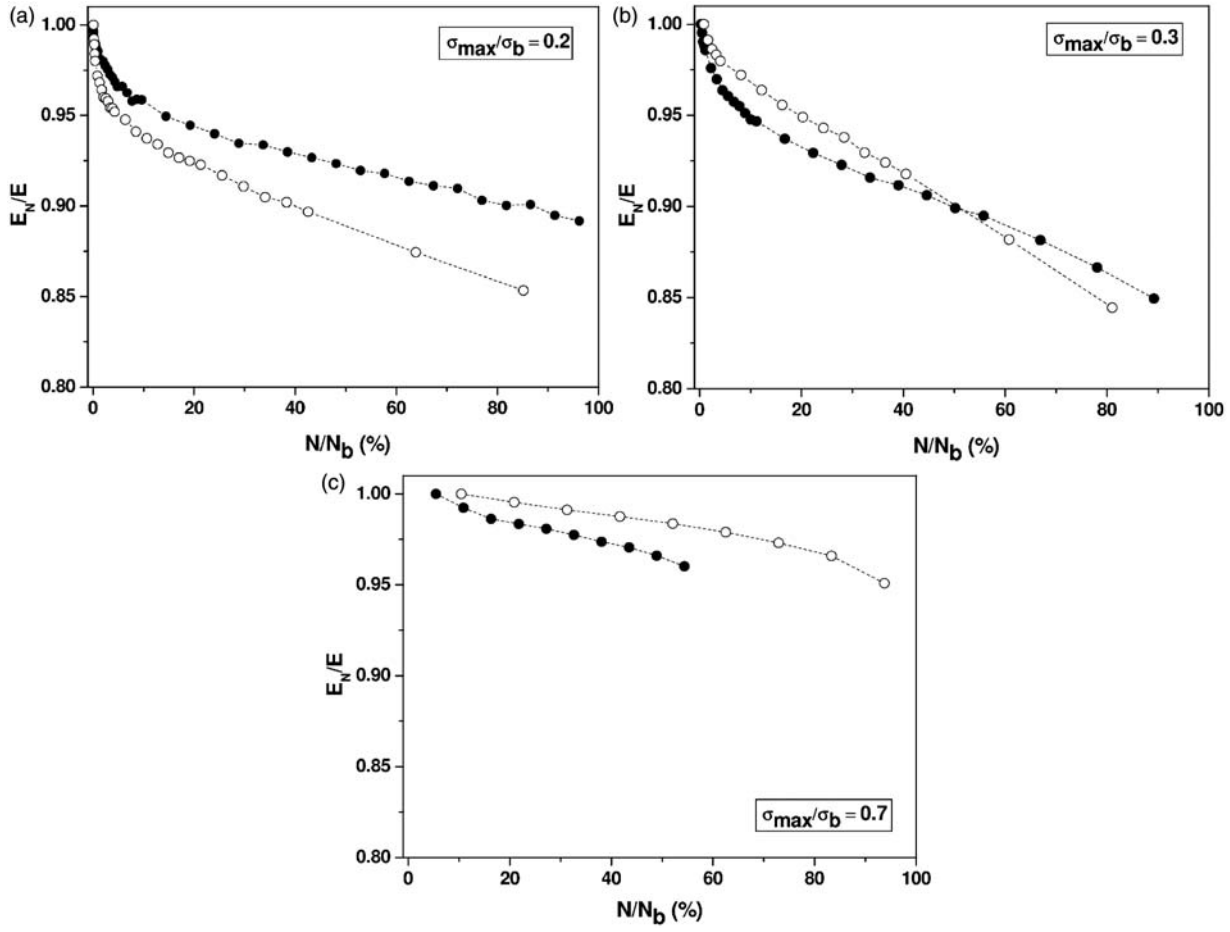

Figure 6. Fatigue behavior of (■) Epoxy-BF200 and (○) Epoxy-BF280 laminates. Relative elastic modulus vs. fatigue life at (a) $\sigma_{max}/\sigma_b = 0.2$, (b) $\sigma_{max}/\sigma_b = 0.3$, and (c) $\sigma_{max}/\sigma_b = 0.7$.

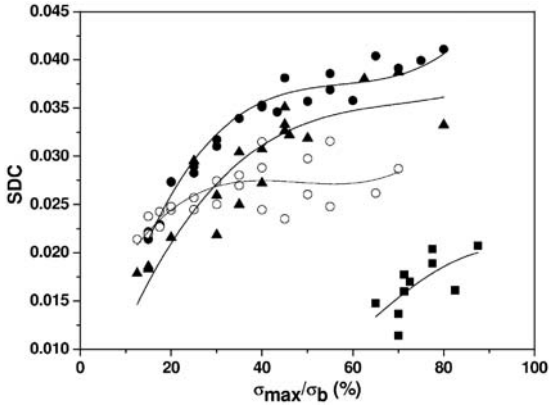

Figure 7. Specific damping capacity (SDC) values of (■) Epoxy-CF200, (●) Epoxy BF200, (▲) Epoxy-GF200, and (○) Epoxy-BF280 laminates.

mechanical and fatigue resistance of BF laminates with respect to GF composites is accompanied by a slightly improved capability to dissipate mechanical energy. It is also possible to correlate changes in damping properties of the investigated materials with their tensile modulus drop at high fatigue loads (see Figure 5). An increase in damping properties is generally associated to an increase in the crack density of the material. Therefore, the higher SDC values observed for Epoxy-BF200 composites with respect to Epoxy-GF200 samples could be probably related to their improved ability to sustain crack propagation and delamination without catastrophic failure. Also, thermal effects due to temperature increase during fatigue tests could explain this behavior, especially for high stress and long times.[72] Considering that BF are generally less conductive than GF[22,24] fibers, it is possible to hypothesize that the local temperature enhancement of Epoxy-BF200 laminate during fatigue tests is more intense than that of the corresponding GF composites, with possible consequences on the energy absorption capability of the materials. However, this is only a hypothesis, and further investigations (i.e. temperature measurements) are needed to assess the role of the temperature variation on the

energy absorption capability of the tested materials. In accordance with stiffness analysis reported in Figure 6, Epoxy-BF200 composite shows higher SDC values with respect to the Epoxy-BF280 sample, especially when an elevated fatigue stress is applied to the material. Once again, the lower void content and the high volume fraction registered for BF200-reinforced laminate is probably responsible for the better damping properties of this laminate, that is able to sustain energy dissipative phenomena (crack nucleation within the matrix and delamination) without the occurrence of catastrophic failure.

Conclusions

Carbon-, basalt-, and E-glass-balanced woven fabrics were utilized for the preparation of epoxy laminates through a hand layup process. Mechanical characterization of laminates reinforced with fabrics having the same areal density demonstrated that BF composites possess an elastic modulus higher than the corresponding glass–fiber laminates, while their tensile strength approaches that of CF samples. The investigation of the fatigue behavior confirmed the better performances of BF laminates with respect to the corresponding glass–fiber composites, with a higher stiffness retention at low fatigue loads and better damping properties. It was therefore highlighted the potential of BF as replacement of traditional GFs for the production of structural composites combining good mechanical performances and interesting energy dissipation capabilities.

Acknowledgments

Mr. Andrea Debortoli is gratefully acknowledged for his support to the experimental work.

References

1. Gay D, Hoa SV and Tsai SW. *Composite materials. Design and applications*. Boca Raton, FL: CRC Press, 2003.
2. Callister WD Jr. *Materials science and engineering*, 3rd ed. New York, NY: John Wiley and Sons, 1994.
3. Czigany T. Trends in fiber reinforcements – the future belongs to basalt fiber. *Express Polym Lett* 2007; 1: 59–59.
4. Kruckenberg TM and Paton R. *Resin transfer molding for aerospace structures*. Dordrecht, The Netherlands: Kluwer, 1998.
5. McCrum NG, Buckley CP and Bucknall CB. *Principles of polymer engineering*. New York, NY: Oxford University Press, 1989.
6. Vladimir K and Vladimir L. Fibres from stone. *Int Textile Bull* 2003; 5: 48–52.
7. Nolf JM. Basalt fibres – fire blocking textiles. *Tech Usage Textil* 2003; 49: 38–42.
8. Saravanan D. Spinning the rocks – basalt fibres. *IE(I) Journal-TX* 2006; 86: 39–45.
9. Milman SB, Velikanova MG and Kotov LE. Developement and study of load bearing heat insulation. *Cryogenics* 1996; 36: 127–130.
10. Wei B, Cao HL and Song SH. Environmental resistance and mechanical performance of basalt and glass fibers. *Mater Sci Eng A – Struct Mater Prop Microstruct Process* 2010; 527: 4708–4715.
11. Subramanian RV and Austin HF. Silane coupling agents in basalt – reinforced polyester composites. *Int J Adhes Adhes* 1980; 1: 50–54.
12. Dias DP and Thaumaturgo C. Fracture toughness of geopolymeric concretes reinforced with basalt fibres. *Cement Concr Compos* 2005; 27: 49–54.
13. Hansen T. Basalt lined ash pipe still in service after nearly four decades. *Power Eng* 2005; 109: 70–71.
14. Novitskii AG and Sudakov VV. An unwoven basalt-fibre material for the encasing of fibrous insulation: an alternative to glass cloth. *Refractor Indust Ceram* 2004; 45: 234–241.
15. Tropina LV, Vasyhk CG, Kornyushina VL, Dyaglev VM, Rassadin YM and Makarushina MA. New cloth from basalt fibres. *Fiber Chem* 1995; 27: 67–68.
16. Sezemanas G, Keriene J, Sinica M, Lankaitis A and Mikulskis D. The alkali and temperature resistance of some fibres. *Mater Sci* 2005; 11: 29–35.
17. Landucci G, Rossi F, Nicolella C and Zanelli S. Design and testing of innovative materials for passive fire protection. *Fire Safety J* 2009; 44: 1103–1109.
18. Czigany T, Poloskei K and Karger-Kocsis J. Fracture and failure behavior of basalt fiber mat-reinforced vinylester/epoxy hybrid resins as a function of resin composition and fiber surface treatment. *J Mater Sci* 2005; 40: 5609–5618.
19. Hu H, Zhang MX, Fangueiro R and de Araujo M. Mechanical properties of composite materials made of 3D stitched woven-knitted preforms. *J Compos Mater* 2010; 44: 1753–1767.
20. Sun BZ, Niu ZL, Zhu LT and Gu BH. Mechanical behaviors of 2D and 3D basalt fiber woven composites under various strain rates. *J Compos Mater* 2010; 44: 1779–1795.
21. Carmisciano S, De Rosa IM, Sarasini F, Tamburrano A and Valente M. Basalt woven fiber reinforced vinylester composites: flexural and electrical properties. *Mater Des* 2011; 32: 337–342.
22. Liu Q, Shaw MT, Parnas RS and McDonnell A-M. Investigation of basalt fiber composite aging behavior for applications in transportation. *Polym Compos* 2006; 27: 475–483.
23. Park JM, Shin WG and Yoon DJ. A study of interfacial aspects of epoxy-based composites reinforced with dual basalt and SiC fibres by means of the fragmentation and acoustic emission techniques. *Compos Sci Technol* 1999; 59: 355–370.
24. Liu Q, Shaw MT, Parnas RS and McDonnell A-M. Investigation of basalt fiber composite mechanical properties for applications in transportation. *Polym Compos* 2006; 27: 41–48.
25. He CH, Li YB, Zhang ZG and Sun ZJ. Impact damage modes and residual flexural properties of composites beam. *J Reinforc Plast Compos* 2008; 27: 1163–1175.

26. Wang M, Zhang Z, Li Y, Li M and Sun Z. Chemical durability and mechanical properties of alkali-proof basalt fiber and its reinforced epoxy composites. *J Reinforc Plast Compos* 2008; 27: 393–407.
27. Cao SH, Wu ZS and Wang X. Tensile properties of CFRP and hybrid FRP composites at elevated temperatures. *J Compos Mater* 2009; 43: 315–330.
28. Mertiny P, Juss K and El Ghareeb MM. Evaluation of glass and basalt fiber reinforcements for polymer composite pressure piping. *J Press Vess-T ASME* 2009; 131: Paper 061407 (6pp.).
29. Dehkordi MT, Nosraty H, Shokrieh MM, Minak G and Ghelli D. Low velocity impact properties of intra-ply hybrid composites based on basalt and nylon woven fabrics. *Mater Des* 2010; 31: 3835–3844.
30. Shokrieh MM and Memar M. Stress corrosion cracking of basalt/epoxy composites under bending loading. *Appl Compos Mater* 2010; 17: 121–135.
31. Tang YS, Wu ZS, Yang CQ, Wu G and Shen S. A new type of smart basalt fiber-reinforced polymer bars as both reinforcements and sensors for civil engineering application. *Smart Mater Struct* 2010; 19: 115001–115014.
32. Wu Z, Wang X, Iwashita K, Sasaki T and Hamaguchi Y. Tensile fatigue behaviour of FRP and hybrid FRP sheets. *Compos Part B: Eng* 2010; 41: 396–402.
33. Ozturk S. The effect of fibre content on the mechanical properties of hemp and basalt fibre reinforced phenol formaldehyde composites. *J Mater Sci* 2005; 40: 4585–4592.
34. Li WD, Cao HL, Chen GR and Shi PF. Preparation and characterization of BF reinforced phenolic resin-based composites. *J Adv Mater* 2010; 42: 67–73.
35. Wang QH, Zhang XR and Pei XQ. Study on the friction and wear behavior of basalt fabric composites filled with graphite and nano-SiO2. *Mater Des* 2010; 31: 1403–1409.
36. Zhang X, Pei X and Wang Q. Friction and wear properties of basalt fiber reinforced/solid lubricants filled polyimide composites under different sliding conditions. *J Appl Polym Sci* 2009; 114: 1746–1752.
37. Cerny M, Glogar P, Sucharda Z, Chlup Z and Kotek J. Partially pyrolyzed composites with basalt fibres – mechanical properties at laboratory and elevated temperatures. *Compos Part A – Appl Sci Manufact* 2009; 40: 1650–1659.
38. Glogar P, Cerny M and Tolde Z. Fracture behaviour of the basalt fibre reinforced composites with polysiloxane-derived matrix. *Acta Geodyn Geomater* 2007; 4: 27–37.
39. Matko S, Anna P, Marosi G, Szep A, Keszei S, Czigany T, et al. Use of reactive surfactants in basalt fiber reinforced polypropylene composites. *Macromol Symposia* 2003; 202: 255–267.
40. Czigany T. Special manufacturing and characteristics of basalt fiber reinforced hybrid polypropylene composites: mechanical properties and acoustic emission study. *Compos Sci Technol* 2006; 66: 3210–3220.
41. Jancar J. Effect of interfacial shear strength on the mechanical response of polycarbonate and PP reinforced with basalt fibers. *Compos Interfaces* 2006; 13: 853–864.
42. Vas LM, Poloskei K, Felhos D, Deak T and Czigany T. Theoretical and experimental study of the effect of fiber heads on the mechanical properties of non-continuous basalt fiber reinforced composites. *Express Polym Lett* 2007; 1: 109–121.
43. Czigany T, Deak T and Tamas P. Discontinuous basalt and glass fiber reinforced PP composites from textile prefabricates: effects of interfacial modification on the mechanical performance. *Compos Interfaces* 2008; 15: 697–707.
44. Kracalik M, Pospisil L, Slouf M, Mikesova J, Sikora A, Simonik J, et al. Recycled poly(ethylene terephthalate) reinforced with basalt fibres: rheology, structure, and utility properties. *Polym Compos* 2008; 29: 437–442.
45. Baets J, Devaux J and Verpoest I. Toughening of basalt fiber-reinforced composites with a cyclic butylene terephthalate matrix by a nonisothermal production method. *Adv Poly Technol* 2010; 29: 70–79.
46. Deak T, Czigany T, Marsalkova M and Militky J. Manufacturing and testing of long basalt fiber reinforced thermoplastic matrix composites. *Polym Eng Sci* 2010; 50: 2448–2456.
47. Deak T, Czigany T, Tamas P and Nemeth C. Enhancement of interfacial properties of basalt fiber reinforced nylon 6 matrix composites with silane coupling agents. *Express Polym Lett* 2010; 4: 590–598.
48. Wittek T and Tanimoto T. Mechanical properties and fire retardancy of bidirectional reinforced composite based on biodegradable starch resin and basalt fibres. *Express Polym Lett* 2008; 2: 810–822.
49. Wittek T and Tanimoto T. Biodegradable starch-based resin reinforced with continuous mineral fibres-processing, characterisation and mechanical properties. *Adv Compos Mater* 2009; 18: 167–185.
50. Chen X, Li Y and Gu N. A novel basalt fiber-reinforced polylactic acid composite for hard tissue repair. *Biomed Mater* 2010; 5: Article Number: 044104 (8pp.).
51. De Rosa I, Marra F, Pulci G, Santulli C, Sarasini F, Tirillò J, et al. Post-impact mechanical characterisation of E-glass/basalt woven fabric interply hybrid laminates. *Express Polym Lett* 2011; 5: 449–459.
52. Wang X, Hu B, Feng Y, Liang F, Mo J, Xiong J, et al. Low velocity impact properties of 3D woven basalt/aramid hybrid composites. *Compos Sci Technol* 2008; 68: 444–450.
53. Deak T and Czigany T. Chemical composition and mechanical properties of basalt and glass fibers: a comparison. *Textile Res J* 2009; 79: 645–651.
54. Weibull W. A statistical distribution function of wide applicability. *J Appl Mech* 1951; 18: 293–297.
55. Gurvich M, Di Benedetto A and Pegoretti A. Evaluation of the statistical parameters of a Weibull distribution. *J Mater Sci* 1997; 32: 3711–3716.
56. Gurev VV, Neproshin EI and Mostovoi GE. The effect of basalt fiber production technology on mechanical properties of fiber. *Glass Ceramics* 2001; 58: 62–65.
57. Detassis M, Pegoretti A and Migliaresi C. Effect of temperature and strain rate on interfacial shear stress transfer in carbon/epoxy model composites. *Compos Sci Technol* 1995; 53: 39–46.
58. Park JM and Subramanian RV. Interfacial shear-strength and durability improvement by monomeric

and polymeric silanes in basalt fiber epoxy single-filament composite specimens. *J Adhes Sci Technol* 1991; 5: 459–477.
59. Park JM, Subramanian RV and Bayoumi AE. Interfacial shear-strength and durability improvement by monomeric and polymeric silanes in single-filament composite specimens of basalt fiber in brittle phenolic and icocyanate resins. *J Adhes Sci Technol* 1994; 8: 133–150.
60. Hofstee J and Van Keulen F. Elastic stiffness analysis of a thermo-formed plain-weave fabric composite Part II: analytical models. *Compos Sci Technol* 2000; 60: 1249–1261.
61. Vassilopoulos AP and Keller T. *Fatigue of fiber-reinforced composites*. London: Springer, 2011.
62. Mandell JF. Fatigue behaviour of short fiber composite materials. In: Reifsnider KL (ed.) *Fatigue of composite materials*. Amsterdam: Elsevier, 1990, pp. 231–337.
63. Mandell JF, Samborsky DD and Cairns DS. *Fatigue of composite materials and substructures for wind turbine blades*. Albuquerque, NM: Sandia National Laboratories, 2002.
64. Chen H-S, Hwang S-F and Chen H-S. Accelerated fatigue properties of unidirectional carbon/epoxy composite materials. *Polym Compos* 2006; 27: 138–146.
65. Chambers AR, Earl JS, Squires CA and Suhot MA. The effect of voids on the flexural fatigue performance of unidirectional carbon fibre composites developed for wind turbine applications. *Int J Fatig* 2006; 28: 1389–1398.
66. Harris B. *Fatigue in composites*. Cambridge: Woodhead Publishing Ltd, 2003.
67. Akynyede O, Mohan R, Kelkar AD and Sankar J. Static and fatigue behavior of epoxy/fiberglass composites hybridized with alumina nanoparticles. *J Compos Mater* 2009; 43: 769–781.
68. Kelkar AD, Tate JS and Bolick R. Structural integrity of aerospace textile composites under fatigue loading. *Mater Sci Eng B* 2006; 132: 79–84.
69. Tate JS, Kelkar AD and Whitcomb JD. Effect of braid angle on fatigue performance of biaxial braided composites. *Int J Fatig* 2006; 28: 1239–1247.
70. O'Brien TK. *Mechanics of nondestructive testing*. New York, NY: Plenum Press, 1980.
71. Chung DDL. *Carbon fiber composites*. Newton, MA: Butterworth-Heinemann, 1994.
72. Razvan A, Bakis CE, Wagnecz L and Reifsnider KL. Infuence of cyclic load ampliutde on damage accumulation and fracture of composite laminates. *J Compos Technol Res* 1988; 10: 3–10.